European Commission

JRC TECHNICAL REPORT

The feasibility of detecting trees affected by the Pine Wood Nematode using remote sensing

Pieter S. A. Beck
Pablo Zarco-Tejada
Peter Strobl
Jesús San Miguel

2015

Report EUR 27290 EN

Joint Research Centre

European Commission
Joint Research Centre
Institute for Environment and Sustainability

Contact information
Pieter S. A. Beck
Address: Joint Research Centre, Institute for Environment and Sustainability, Via E. Fermi 2749, I-21027 Ispra, Italy
E-mail: pieter.beck@jrc.ec.europa.eu
Tel.: +39 0332 78 3671

JRC Science Hub
https://ec.europa.eu/jrc

JRC 95972

EUR 27290 EN

ISBN 978-92-79-48946-4

ISSN 1831-9424

doi: 10.2788/711975

Luxembourg: Publications Office of the European Union, 2015

Abstract

At the request of DG SANTE, the Joint Research Centre conducted a pilot study between November 2014 and April 2015 to establish the feasibility of the remote-sensing-based detection of trees affected by Pine Wood Nematode (PWN) in the 2.2 Mha buffer zone established along the Portugal-Spain border. The JRC collected multiple types of remote sensing data at various resolutions from a range of sensors on aircraft and satellites over a 7 000-ha study site in Spain during the winter of 2014-2015. The images were evaluated for their ability to distinguish a) between pine trees that appeared to have a healthy canopy, and those showing decline, and b) between different levels of canopy decline, in terms of defoliation, decolouration and die-off. Detailed analysis of the imagery showed that properly processed remote sensing observations, particularly at high spatial and spectral resolution from aircraft, can help identify pine trees showing canopy decline. The ability to detect individual tree crowns and varying levels of canopy decline varied with the image resolution, the type of sensor used to acquire the data, and the level of processing of the data. This report uses the findings of the study to spell out a set of technical recommendations for the operational monitoring of tree canopy health over large areas in the context of tree pest outbreaks.

Contents

1. Executive Summary

At the request of DG SANTE[1], the Joint Research Centre conducted a pilot study between November 2014 and April 2015 to establish the feasibility of the remote-sensing-based detection of trees affected by Pine Wood Nematode (PWN) in the 2.2 Mha buffer zone established along the border between Portugal and Spain. This report describes the study, and the conclusions drawn from it regarding the feasibility of operationally monitoring the trees in the buffer zone for Pine Wilt Disease symptoms using remote sensing.

After consulting the Portuguese and Spanish authorities, the site for the pilot study was placed in a 7 000-ha pine forest in northern Extremadura, Spain. This area is free of Pine Wood Nematode, but was surveyed by local authorities for pine trees with canopy decline symptoms similar to those caused by nematodes.

In the winter of 2014-2015, the JRC collected multiple types of remote sensing data over the study site, from both aircraft and satellites, using a range of sensors and resolutions. The images were evaluated for their ability to distinguish a) between pine trees that appeared to have a healthy canopy and those showing decline, and b) between different levels of canopy decline, in terms of defoliation, decolouration and die-off. Detailed analysis of the imagery showed that remote sensing observations, particularly at high spatial and spectral resolution from aircraft, can help identify pine trees that show canopy decline. The ability to detect individual tree crowns and varying levels of canopy decline varied with the image resolution, the type of sensor used to acquire the data, and the level of processing of the data. The study led to the following recommendations:

[REC.1] To provide a detailed record of individual coniferous tree crowns in the buffer zone, the area should be imaged in colour at 20-cm or higher spatial resolution from manned airborne platforms.

[REC.2] Images acquired for forest monitoring in the context of the PWN emergency should be of very high quality in terms of georegistration to ensure that, once repeat imagery is available, changes can be detected as close to the individual crown level as possible.

[REC. 3] In an attempt to detect lower levels of canopy decline, a multispectral narrow-band sensor should image areas of interest from the same aircraft and at the same time as broad-band colour images are acquired, at the highest spatial resolution achievable.

[REC. 4] Thermal imaging of pine forests with early stages of canopy decline should be conducted in summer when plants are under water stress, in order to evaluate in more detail the ability of thermal images to detect canopy decline earlier than optical imagery can.

[REC. 5] To attain the highest cartographic precision possible in collected imagery, the best available high resolution digital elevation models and existing catalogues of aerial

[1] Ares(2014)3349156

orthophotographs of the area to be surveyed should be used for the orthorectification and geometric rectification of newly acquired imagery.

[REC. 6] Output from remote sensing analyses should be made available in GIS-compatible digital formats. Up-to-date information from field observations, laboratory analyses, and felling operations should be accessible during the analysis of remote sensing imagery so that output can be validated, and methods progressively refined.

[REC. 7] An initial phase of operational monitoring of the PWN buffer zone should aim to obtain wall-to-wall imaging of priority areas, in order to allow for the mapping of all individual coniferous tree stands in those areas. In a second phase of operational monitoring, once individual trees have been mapped, flight paths could then be planned together with complementary ground surveys, to optimise cost efficiency of the monitoring exercise.

This pilot study established that it is feasible to reliably detect pine trees showing severe canopy decline from remote sensing in a landscape similar to that found in the PWN buffer zone. It provides clear recommendations for more operational remote-sensing-based forest monitoring activities in the context of PWN, as well as for continued research into cost-efficient methods. At 2.2 Mha, the PWN buffer zone is large, and an exceptionally large volume of image data needs to be acquired and processed in order to exhaustively monitor the area for declining trees. We therefore suggest that, in a next phase, the operationalisation of tree decline detection techniques adopt the abovementioned recommendations and be progressively developed over an area that is significantly larger than that of the pilot study area (from 10 000 to 100 000 ha), but still smaller than the entire buffer, so as to reduce the significant risk of scaling up the operations too quickly. The area for this phase of monitoring should be chosen in a priority region of the buffer zone, e.g. closest to the current Pine Wood Nematode distribution, in order for results to have immediate forest management value.

The technical challenges faced by efforts to detect trees with declining canopies, as detailed in the present study, are not unique to the Pine Wood Nematode case. Indeed, they can form the basis for a versatile remote-sensing-based toolkit to monitor forest health in the fight against tree pests. Research is currently being carried out in several Member States to detect pest disturbances in forest stands. However, given the extent and rate at which pests are currently spreading (e.g. the ongoing outbreak of *Xylella fastidiosa* in southern Italy), and the threat of pests spreading from one Member State into another, a pan-European early warning system for forest health would have significant benefits.

2. Motivation for this study

EU rules on quarantine pests are in place to protect plants against harmful pests and diseases, by preventing their introduction into and further spread within the EU. Council Directive 2000/29/EC [2] provides the general framework which lays down provisions on imports of plants and plant products, movement of plants, eradication and containment measures in case of outbreaks, as well as the possibility to recognise protected zones free from certain quarantine pests.

For a number of quarantine organisms, EU emergency measures are in place to prevent their further introduction into and spread within the Union. One of these harmful organisms is the Pine Wood Nematode (PWN, *Bursaphelenchus xylophilus*), regarded as one of the five most harmful biotic agents for EU forests[3]. PWN made its way into the European Union in 1999 and has since spread through a large portion of Portugal, killing predominantly maritime pine trees (*Pinus pinaster*). In the context of this ongoing outbreak, a 2.2 Mha buffer zone is established in Portugal along its entire border with Spain. As required by Commission Implementing Decision 2012/535/EU[4], the buffer zone surrounds the infected zone where PWN is found to be present. Within the buffer zone, one of the key control measures to be performed outside the flight season of the vector, before the next flight season, is the identification, felling and proper disposal of all trees susceptible to PWN which are dead, in poor health or situated in fire or storm affected areas. In accordance with the EU Decision, also susceptible trees which are identified in declining conditions during the flight season of the vector shall immediately be felled and properly disposed of. In order to achieve this, the entire 2.2 Mha area has to be surveyed exhaustively for individual trees showing canopy decline symptoms. In July 2014, the European Commission's Directorate-General for Health and Food Safety (then DG SANCO, now DG SANTE) contacted the Forest Resources and Climate Unit of the Joint Research Centre (JRC) to express their interest in establishing whether it would be possible to exhaustively monitor the buffer zone for coniferous trees that show symptoms of canopy decline using remote sensing. This report describes a pilot study undertaken between November 2014 and April 2015 by the JRC to establish the feasibility of using remote sensing to detect trees affected by PWN.

3. Pilot study site

The pilot study site, Monte de Granadilla, is situated in the north of the Extremadura region of Spain, and about 60 km from the border with Portugal. The area is managed by the Organismo Autónomo de Parques Nacionales, which falls under the Ministerio de Agricultura, Alimentación y Medio Ambiente. The entire area comprises approximately 7 000 ha of pine forest, with *Pinus pinaster*, *Pinus pinea*, and *Pinus nigra* occurring in both mixed stands and stands dominated by a single species. *Pinus nigra* is mostly found at higher elevations. Most of the pine stands in the area were planted in the 1960s, and thinned in 2009. Elevations range from circa 370 m a.s.l. along the shores of the Gabrile y Galán reservoir in the southwest, to circa 1 000 m in the northeast of the forest area.

[2] http://eur-lex.europa.eu/LexUriServ/LexUriServ.do?uri=OJ:L:2000:169:0001:0112:EN:PDF

[3] ec.europa.eu/environment/forests/pdf/FBD_report_2012.pdf

[4] http://eur-lex.europa.eu/LexUriServ/LexUriServ.do?uri=OJ:L:2012:266:0042:0052:EN:PDF

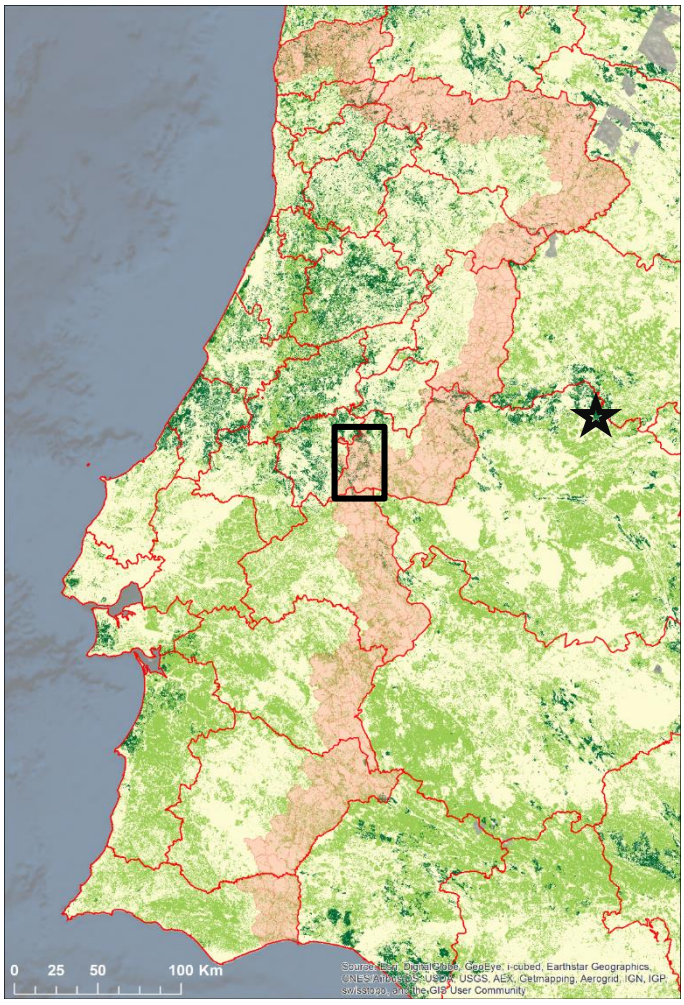

Figure 1. Map of Portugal showing (in pink) the 2.2 Mha buffer zone established along its border with Spain to prevent the spread of PWN. The background map shows coniferous forests (dark green), deciduous forests (light green), and non-forested areas (yellow). The black rectangle indicates the area used for a flight cost simulation (see section 5.5), and the star shows the location of the Monte de Granadilla forest - the study area surveyed both directly in the field, and remotely from aircraft and satellite for the presence of pine trees that show canopy decline.

4. Data collected

4.1. Ground survey

On and around 20 November 2014, local authorities surveyed 293 pine trees in the Monte de Granadilla forest for size and canopy condition. The survey targeted dominant trees showing canopy decline, where dominant trees are those that have attained or have the potential to attain maximum height and crown development.

The location of each tree was initially registered using a hand-held GPS, along with the following measurements:

Metric	Units	Notes
Size		
Diameter at breast height	cm	
Projected crown size	m	
Height	m	
Crown condition		
Defoliation	6 intervals: < 11% < 26% < 41% < 61% < 100% 100%	Defoliated states included: • smaller branches and branchlets that should be carrying needles, but aren't • needles that have shed prematurely • **dry needles, which are brown or reddish**
Discolouration	6 intervals: < 11% < 26% < 41% < 61% < 100% 100%	Colour anomalies in **live** needles: • Colour anomalies were considered with reference to species, season, and site, and using reference trees • Discolouration classes are assigned based on the overall hue of the live crown • **Very localised strong discolouration in the crown is not considered**
Canopy die-off	6 intervals: < 1% < 26% < 51% < 76% < 100% 100%	Large dead branches that have lost their needles and sprouts years ago are not considered, as they represent historical die-off and have no direct bearing on the current status of the tree

Table 1. Properties of selected pine trees recorded during the ground survey in the Monte de Granadilla forest.

About half of the trees surveyed had projected crown diameters of < 2 m, while 10% of the trees had crown diameters that were > 4.5 m. Most trees were between 5 and 10 m tall, with the tallest tree surveyed measuring 15 m in height (*Figure 2*).

The survey did not include any trees that were considered to be completely healthy, i.e. those simultaneously belonging to the lowest classes for defoliation, discolouration, and canopy die-off. To overcome this, the set of trees surveyed in the field was complemented by a set of 30 apparently healthy trees (i.e. that did not show any canopy decline symptoms) identified using very high resolution imagery acquired from aircraft.

Canopy die-off of the trees surveyed in the field followed a strongly bimodal distribution. About 60% (182/293, **Figure 3**) of the trees in the survey had completely dead crowns (Canopy die-off = 100%, e.g. **Figure 4a**). Only one tree had canopy die-off of between 50% and 100%, with the 111 remaining trees showing less than 51% of canopy die-off (e.g. **Figures 4b, 4c, and 4d**). Most of the trees with incomplete die-off had >60% of both defoliation and discolouration (**Figure 3**). 40 trees (14% of the trees surveyed) had less than 1% canopy die-off. Four of the surveyed trees fell into the lowest defoliation interval (<11% defoliation). These trees had no canopy die-off, but were completely discoloured. Only one surveyed tree fell into the lowest discolouration interval (<11% discolouration).

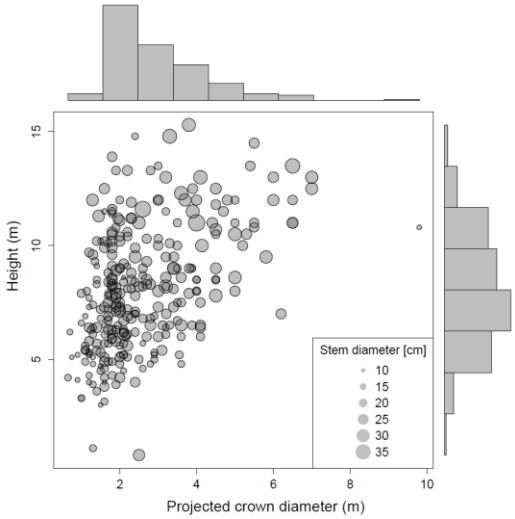

Figure 2. Heights, stem diameters, and projected crown diameters of the 293 trees surveyed for this study in the Monte de Granadilla forest.

	Interval 1	Interval 2	Interval 3	Interval 4	Interval 5	Interval 6
Defoliation	4	6	2	18	76	187
Discolouration	1	4	8	16	72	192
Canopy die-off	40	59	10	1	0	183

Table 2. Number of trees observed in severity intervals for the three canopy decline characteristics included in the field survey. For a description of the intervals, see Table 1.

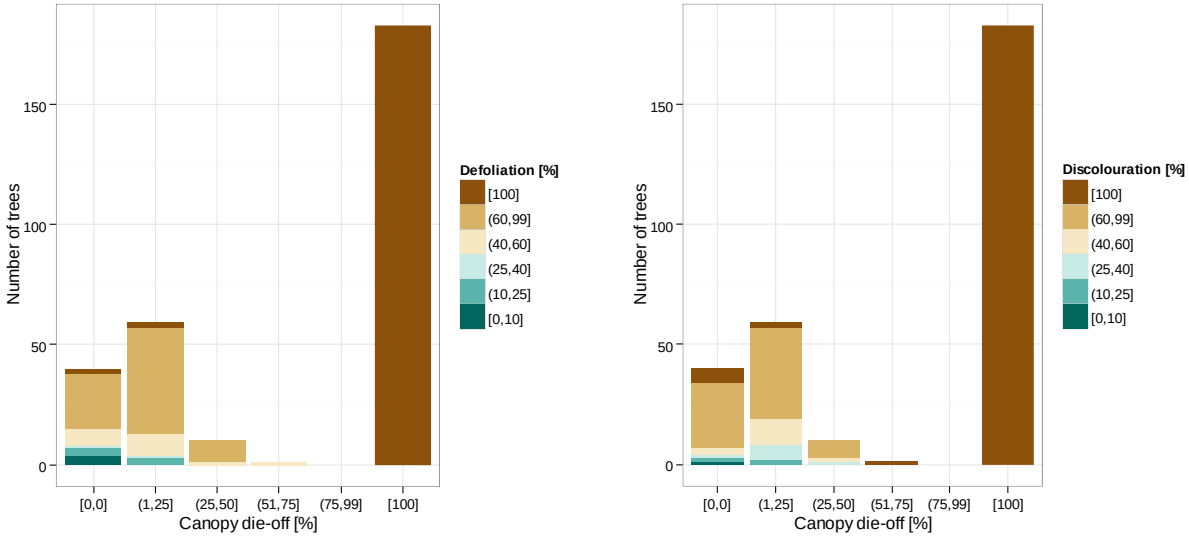

Figure 3. Distribution of defoliation (left panel) and discolouration (right panel) classes observed in trees displaying increasing levels of canopy die-off.

A) Crown size: 3.2 m, Height: 8.2 m, Defoliation: 100%, Discolouration: 100%, Canopy die-off: 100%

B) Crown size: 1.7 m, Height: 6.8 m, Defoliation < 26%, Discolouration: 100%, Canopy die-off: 0%

C) Crown size: 2 m, Height: 7.1 m, Defoliation < 100%, Discolouration < 100%, Canopy die-off: 0%

D) Crown size: 2.7, Height: 9.3 m, Defoliation: < 100%, Discolouration: < 100%, Canopy die-off: < 26%

Figure 4. Examples of four trees surveyed in the field, with their crown condition observations.

4.2. Aerial images

4.2.1. Colour images and False-Colour/Near-Infrared (FCNI) images

The colour and false-colour/near-infrared (FCNI) images were recorded by a full-frame Digital Single Lens Reflex (DSLR) camera. Standard DSLR cameras have a filter that prevents

near-infrared light from reaching the sensor. To record the FCNI images, a standard DSLR camera was modified to remove the near-infrared filter, such that it recorded green, red, and near-infrared radiance, as opposed to the Red-Green-Blue recordings of the standard (natural) colour set-up.

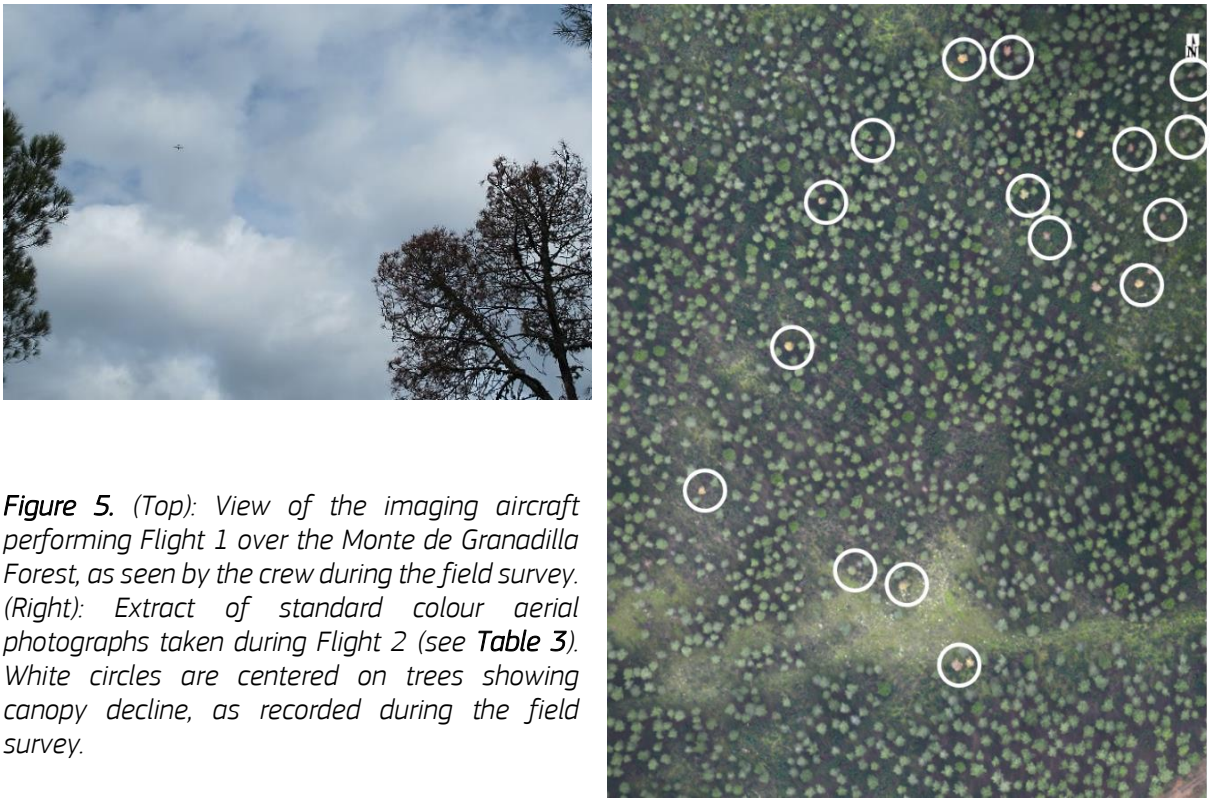

Figure 5. (Top): View of the imaging aircraft performing Flight 1 over the Monte de Granadilla Forest, as seen by the crew during the field survey. (Right): Extract of standard colour aerial photographs taken during Flight 2 (see Table 3). White circles are centered on trees showing canopy decline, as recorded during the field survey.

	Flight 1	**Flight 2**	**Flight 3**
Date	20/11/2014	02/12/2014	28/01/2015
Weather conditions	cloudy (Figure 5, top)	partially cloudy	cloud-free
Area imaged	3 000 ha	3 000 ha	surveyed trees only
Flight altitude above sea-level	4 260 ft	4 260 ft	3 000 ft
Flight altitude above ground	550-850 m	550-850 m	200-450 m
Sensors & image resolution			
Colour	11 cm	--	--
False-colour / near-infrared (FCNI)	--	--	20 cm
Hyperspectral	70 cm	70 cm	40 cm
Thermal	80 cm	80 cm	50 cm

Table 3. Overview of flights conducted as part of the pilot study, and remote sensing data acquired. All flights were conducted at a heading that was coincident with the solar plane (335°).

4.2.2. Hyperspectral images

The hyperspectral images recorded radiance between wavelengths of 400 nm and 1 000 nm, in 1.85 nm intervals, generating 260 records for each pixel. For comparison, an RGB image contains three records per pixel: Red, Green, and Blue. Data were recorded in 12-bit format, and have a theoretical signal-to-noise ratio of 300:1.

Prior to deployment, the hyperspectral sensor was first calibrated in the laboratory in order to determine how digital values registered by the sensor can be transformed to radiance values for each recorded wavelength. The resulting calibration functions allowed for the generation of hyperspectral radiance images (expressed in W m^{-2} $micron^{-1}$ sr^{-1}) from the sensor's raw measurements.

4.2.3. Thermal images

The thermal images were acquired using an infrared camera that recorded data in 16-bit format and a theoretical temperature sensitivity of less than 50 mK. The thermal camera was also calibrated in the laboratory prior to field operations. The relationship between the digital values recorded by the camera and actual temperatures was established by calibrating the instrument to view a reference object with a very precisely controlled temperature (a 'black body instrument').

4.2.4. Satellite images

In addition to the aerial images, commercial high-resolution satellite images of the Monte de Granadilla forest area were acquired in order to evaluate whether they could provide an alternative to monitoring from airborne platforms (*Table 4*).

	Image 1	**Image 2**	**Image 3**
Date	30/05/2010	25/04/2013	26/05/2014
Sensor	WorldView 2	WorldView 2	Pleiades
MS bands	8	8	4
MS resolution	2 m	2 m	2 m
PAN resolution	50 cm	50 cm	50 cm

Table 4. Overview of satellite data purchased as part of the pilot study, including the spatial resolution of their multispectral (MS) and the panchromatic (PAN) images.

4.3. Map data

To evaluate the presence of coniferous forest in the buffer zone, we used the Forest Type maps that were recently produced for the Copernicus Land Monitoring Services (http://land.copernicus.eu/pan-european/high-resolution-layers/forests). These maps depict the distribution of deciduous forest areas, coniferous forest areas, and non-forest areas, at 25-m resolution. The Portuguese authorities provided the outline of the buffer zone, and the administrative units that constitute it.

5. Data Analysis

5.1. Image preprocessing

The following section gives a short description of the image preprocessing steps that must be followed before features (e.g. tree or forest stands) in remote sensing data can be analysed quantitatively.

These steps pertain to the geographical registration of the images in order to produce maps from the data (section 5.1.1), the correction for variation in atmospheric and illumination conditions in order to compare images acquired on different days or different times of day (section 5.1.2), and to the mosaicing of individual images acquired during the flights in order to provide coherent wall-to-wall views of the entire area surveyed (see *Figure 6*).

5.1.1. Orthorectification

Images acquired from different remote sensing platforms do not naturally align, because the view they provide of the Earth's surface depends on the flight height, the field of view of the sensor, and the topography of the terrain. To eliminate these differences in perspective and terrain, images are 'orthorectified' so that they all align cartographically. Orthorectification is performed using a digital elevation model (DEM), which describes the terrain surveyed, the position and internal geometry of the sensor used to quantify the image perspective and distortion, and often a reference image. Where the latter is included, common features of the new and the reference image are identified and used to fine-tune the image-to-image alignment.

In this study, both the aerial and satellite images were orthorectified using the 10-m-resolution Spanish national reference DEM, provided by Spain's Instituto Geográfico Nacional (IGN). As reference images, we used the orthorectified aerial photographs made available through IGN's Plan Nacional de Ortofotografía Aérea (PNOA) portal. The photos are available through the web maps service: http://www.ign.es/wms-inspire/pnoa-ma?

5.1.2. Atmospheric correction

Images acquired by remote sensing record the Earth's surface, but are also influenced by the sensor design, and the position of the sun and the sensor with respect to each other and to the surface. The satellite images used in this study were processed to account for differences in sun-surface-sensor geometry and (extra-atmospheric) solar irradiance. This calculation of "top of atmosphere" reflectance data facilitates the comparison of images.

Remote sensing data are also influenced by the atmospheric conditions that prevailed at the time of the flight. Eliminating atmospheric effects from the data aids the comparison of images acquired on different dates, or at different times of day. The hyperspectral images collected for this study were corrected for atmospheric influences using a radiative transfer model that simulates how light travels under different atmospheric conditions. The model used in-situ measurements that record the solar radiation reaching the surface at different wavelengths at the time of the flight. By comparing these measurements to the solar radiation hitting the outside of the Earth's atmosphere, which is calculated based on the time of day and geographical position, the model simulates how the prevailing atmospheric conditions influence the aircraft observations at different wavelengths. Ultimately, this modelling effort permits the calculation of "surface reflectance" - the proportion of light reflected by the surface, irrespective of the atmospheric conditions.

Figure 6. Example of a mosaic of very high resolution colour imagery acquired over the Monte de Granadilla forest before (top) and after (bottom) the difference in sensor illumination when the aircraft is flying towards or away from the sun. The diagonal banding in the top image coincides with the flight lines the aircraft followed in alternating directions to obtain images of the entire study area. The depicted area measures 2.5 km across.

5.2. Tree crown identification and delineation

At the edge of its distribution, Pine Wilt Disease often affects individual trees in otherwise healthy stands. For remote sensing to help detect these trees, all trees need to be first identified in the imagery and then individually evaluated for evidence of decline, as they are unlikely to show up in stand-level analyses of remote sensing imagery. This requirement motivated the acquisition of very high resolution data for the study. Once preprocessing of the imagery was complete, we developed semi-automatic routines for the delineation of individual tree crowns in the imagery. The resulting geospatial database of tree crowns provides a detailed map of the distribution of trees in the study area, which aids the planning of future surveys in the field and from the air. Furthermore, the delineation of tree crowns in the maps ensures that understory vegetation and soils do not hinder the canopy analysis using the spectral information in the imagery.

Tree crowns can be detected in aerial images based on their spectral features or their typical shape. 'Segmentation' approaches divide an image into homogenous polygons ('segments') that fulfil pre-defined shape, size, and texture criteria. Segments are then commonly classified based on their spectral characteristics, in order to identify objects of interest, such as tree crowns. However, in our case, the spectral signature of tree crowns, and particularly of those with decline symptoms, are not known a priori. Furthermore, even if spectral profiles

of coniferous trees were known over a gradient of crown status, actual spectral values in very high resolution imagery will vary considerable between scenes acquired at different times, owing to the difficulty of correcting them completely for variations introduced by atmospheric and illumination conditions. Therefore, the segment-and-classify approach runs the risk that trees with decline symptoms go undetected. To minimise this risk, we opted for an alternative two-step approach: In the first step, the centre of each tree crown was identified by visual inspection of the imagery, and marked as a point. In the second step, an automated 'region growing' algorithm detected and outlined spectrally homogenous crown shapes around these points.

5.3. Spectral analyses

Once individual tree crowns were mapped, we aimed to evaluate whether progressive stages of canopy decline could be discerned using the remote sensing observations. Since hyperspectral data contains the greatest degree of spectral detail of all the reflectance datasets, it is best suited to calculate a variety of spectral indices that are sensitive to biophysical status and process because of the way these influence reflectance, in particular electromagnetic wavelengths. *Table 5* summarises the 59 spectral indices evaluated in this study. While a detailed description of each of these is beyond the scope of this report, they generally fall into six groups:

1. **Structural indices** are sensitive to vegetation structure, growth, canopy volume and density. These are expected to be change with to canopy damage and areas of low plant vigour, but are not expected to detect symptoms invisible to the naked eye.
2. **Pigment indices** are sensitive to the degradation of pigments involved in the photosynthetic cycle, e.g. chlorophylls and carotenoids.
3. The **Photochemical Reflectance Index** (PRI) is an indicator of stress in plants, including water stress. It is influenced by the epoxidation of the xanthophylls, which itself varies with light-use efficiency, or the rate at which plants can absorb carbon for a given amount of energy, i.e. light, absorbed.
4. Similarly, reduced photochemical efficiency due to water stress can result in Chlorophyll fluorescence, i.e. the re-emission, in particular wavelengths, of absorbed sunlight by chlorophyll, an effect measured by **Chlorophyll fluorescence indices**. As such, xanthophyll- and fluorescence-related indices are hypothesised to detect stress in the canopy earlier than structural or photosynthetic pigment indices would.
5. **Colour indices** quantify changes in the colour of canopies in the visible wavelengths. They differ from the indices that can be calculated from standard colour or colour-NIR imagery in that they are based on a more specific part of the electromagnetic spectrum in the visible range. By comparing colour indices generated from hyperspectral and standard RGB imagery, we can evaluate whether (more challenging) narrow-band hyperspectral imaging provides an added value in detecting canopy decline. Therefore, we calculated the following indices using the standard colour images and the FCNI:
    - colour imagery indices: R; G; B; R/G; R/B; G/B
    - FCNI imagery: G; R; NIR; G/R; G/NIR; R/NIR
6. We also evaluated a recently published **Plant disease index** that, in an experimental study, performed best among all possible normalised band ratios at detecting

different levels of *Cercospora* leaf spot, sugar beet rust, and powdery mildew in sugar beet leaves.

Besides these 59 indices based on reflectance in visible and near-infrared wavelengths, which could indicate structural changes in the canopy and elevated stress levels, we also analysed whether different degrees of canopy decline were detectable in the crown temperatures shown by the **thermal observations**. Canopy temperature is one of the most widely used physiological indicators of water stress. In the case of Pine Wilt Disease, the obstruction of sap flow in the xylem by nematodes reduces the availability of water in the crown, and with it the potential for transpiration. Particularly during times of high evaporative demand in the atmosphere, i.e. on hot and dry days, Pine Wilt Disease and other stressors of plant hydrology prevent transpiration, which has a cooling effect on the canopy. As this latent heat flux from the crown to the atmosphere is reduced under water stress, energy instead enters a sensible heat flux, which causes the canopy temperature to increase.

Vegetation indices	**Abbreviation and calculation**	**Ref.**
Structural indices		
Normalized Difference Vegetation Index	$NDVI = (R_{800} - R_{670})/(R_{800} + R_{670})$	1
Renormalized Difference Vegetation Index	$RDVI = (R_{800} - R_{670})/\sqrt{(R_{800} + R_{670})}$	2
Simple Ratio	$SR = R_{800}/R_{670}$	3
Modified Simple Ratio	$MSR = \frac{R_{800}/R_{670} - 1}{(R_{800}/R_{670})^{0.5} + 1}$	4
Optimised Soil-Adjusted Vegetation Index	$OSAVI = ((1 + 0.16) \cdot (R_{800} - R_{670})/(R_{800} + R_{670} + 0.16))$	5
Modified Soil-Adjusted Vegetation Index	$MSAVI = \frac{2 \cdot R_{800} + 1 - \sqrt{(2 \cdot R_{800} + 1)^2 - 8(R_{800} - R_{670})}}{2}$	6
Triangular Vegetation Index	$TVI = 0.5 \cdot [120 \cdot (R_{750} - R_{550}) - 200 \cdot (R_{670} - R_{550})]$	7
Modified Triangular Vegetation Index 1	$MTVI1 = 1.2[1.2(R_{800} - R_{550}) - 2.5(R_{670} - R_{550})]$	8
Modified Triangular Vegetation Index 2	$MTVI2 = \frac{1.5[1.2(R_{800} - R_{550}) - 2.5(R_{670} - R_{550})]}{\sqrt{(2R_{800} + 1)^2 - (6R_{800} - 5\sqrt{R_{670}}) - 0.5}}$	8
Modified Chlorophyll Absorption Ratio Index 1	$MSAVI1 = 1.2[2.5(R_{800} - R_{670}) - 1.3(R_{800} - R_{550})]$	8
Modified Chlorophyll Absorption Ratio Index 2	$MSAVI2 = \frac{1.5[2.5(R_{800} - R_{670}) - 1.3(R_{800} - R_{550})]}{\sqrt{(2R_{800} + 1)^2 - (6R_{800} - 5\sqrt{R_{670}}) - 0.5}}$	8
Enhanced Vegetation Index	$EVI = 2.5 \cdot (R_{800} - R_{670})/(R_{800} + 6 \cdot R_{670} - 7.5 \cdot R_{400} + 1)$	9
Lichtenthaler index	$LIC1 = (R_{800} - R_{680})/(R_{800} + R_{680})]$	10
Pigment indices		
Vogelmann indices	$VOG1 = R_{740}/R_{720}$	11
	$VOG2 = (R_{734} - R_{747})/(R_{715} + R_{726})$	12
	$VOG3 = (R_{734} - R_{747})/(R_{715} + R_{720})$	12
Gitelson & Merzlyak indices	$GM1 = R_{750}/R_{550}$	
	$GM2 = R_{750}/R_{700}$	13
Transformed Chlorophyll Absorption in Reflectance Index	$TCARI = 3 \cdot [(R_{700} - R_{670}) - 0.2 \cdot (R_{700} - R_{550}) \cdot (R_{700}/R_{670})$	14
Transformed Chlorophyll Absorption in Reflectance Index/ Optimised Soil-Adjusted Vegetation Index	$\frac{TCARI}{OSAVI} = \frac{3 \cdot [(R_{700} - R_{670}) - 0.2 \cdot (R_{700} - R_{550}) \cdot (R_{700}/R_{670})}{((1 + 0.16) \cdot (R_{800} - R_{670})/(R_{800} + R_{670} + 0.16))}$	14
Chlorophyll index red edge	$CI = R_{750}/R_{710}$	14
Simple Ratio Pigment Index	$SRPI = R_{430}/R_{680}$	15
Normalized Phaeophytinization Index	$NPQI = (R_{415} - R_{735})/(R_{415} + R_{735})$	15
Normalized Pigments Index	$NPCI = (R_{680} - R_{430})/(R_{680} + R_{430})$	16
Carter indices	$CTRI1 = R_{695}/R_{420}$	17
	$CAR = R_{695}/R_{760}$	17

Reflectance band ratio indices	$Datt - CabCx + c = R_{672}/(R_{550} \cdot 3R_{708})$	
	$DattNIRCabCx + c = R_{860}/(R_{550} \cdot R_{708})$	18
Structure-Intensive Pigment Index	$SIPI = (R_{800} - R_{445})/(R_{800} + R_{680})$	16
Carotenoid Reflectance Indices	$CRI_{550} = (1/R_{515}) - (1/R_{550})$	19
	$CRI_{700} = (1/R_{515}) - (1/R_{700})$	19
	$RNIR \cdot CRI_{550} = (1/R_{510}) - (1/R_{550}) \cdot R_{770}$	19
	$RNIR \cdot CRI_{700} = (1/R_{510}) - (1/R_{700}) \cdot R_{770}$	19
Plant Senescing Reflectance Index	$PSRI = (R_{680} - R_{500})/R_{750}$	20
Lichtenhaler index	$LIC3 = R_{440}/R_{740}$	21
Ratio analysis of reflectance spectra	$RARS = R_{746}/R_{513}$	22
Pigment Specific Simple Ratio Chlorophyll a	$PSSRa = R_{800}/R_{675}$	23
Pigment Specific Simple Ratio Chlorophyll b	$PSSRb = R_{800}/R_{650}$	23
Pigment Specific Simple Ratio Carotenoids	$PSRRc = R_{800}/R_{500}$	23
Pigment Specific Normalized Difference	$PSNDc = (R_{800} - R_{470})/(R_{800} + R_{470})$	24
Photochemical reflectance indices		
Photochemical Reflectance Index (570)	$PRI_{570} = (R_{570} - R_{531})/(R_{570} + R_{531})$	25
Photochemical Reflectance Index (515)	$PRI_{515} = (R_{515} - R_{531})/(R_{515} + R_{531})$	26
Photochemical Reflectance Index (512)	$PRI_{m1} = (R_{512} - R_{531})/(R_{512} + R_{531})$	26
Photochemical Reflectance Index (600)	$PRI_{m2} = (R_{600} - R_{531})/(R_{600} + R_{531})$	27
Photochemical Reflectance Index (670)	$PRI_{m3} = (R_{670} - R_{531})/(R_{670} + R_{531})$	27
Photochemical Reflectance Index (670 and 570)	$PRI_{m4} = (R_{570} - R_{531} - R_{670})/(R_{570} + R_{531} + R_{670})$	26
Normalized Photochemical Reflectance Index	$PRI_n = \frac{PRI_{570}}{RDVI \cdot (R_{700}/R_{670})})$	28
Carotenoid/chlorophyll ratio index	$PRI \cdot CI = (R_{680} - R_{500})/R_{750}$	29
Chlorophyll Fluorescence indices		
Reflectance Curvature Index	$CUR = (R_{675} \cdot R_{690})/R_{683}^2$	30
Colour indices		
Redness index	$R = R_{700}/R_{670}$	31
Greenness index	$G = R_{570}/R_{670}$	32
Blue index	$B = R_{450}/R_{490}$	32
Blue/green indices	$BGI1 = R_{400}/R_{550}$	33
	$BGI2 = R_{450}/R_{550}$	33
Blue/red indices	$BRI1 = R_{400}/R_{690}$	34
	$BRI2 = R_{450}/R_{690}$	34
Red/green index	$RGI = R_{690}/R_{550}$	33
Lichtenthaler index	$LIC2 = R_{440}/R_{690}$	35
Plant disease index		
Health index	$HI = \frac{(R_{534} - R_{698})/}{R_{534} + R_{698}} - \frac{1}{2} \cdot R_{704}$	36

Table 5. Vegetation indices calculated from hyperspectral imagery for detected tree crowns, and evaluated for their ability to detect canopy decline. In the 'Abbreviation and Calculation' column, R_n refers to the reflectance measured at a wavelength of n nm. See Calderon et al. (2013, doi:10.1016/j.rse.2013.07.031) for references and a description of many of these indices in the framework of verticillium wilt detection in olive orchards. References (Ref.): 1=Rouse et al. (1974), 2=Rougean and Breon (1995), 3=Jordan (1969), 4=Chen (1996), 5=Rondeaux et al. (1996), 6=Qi et al. (1994), 7=Broge and Leblanc (2000), 8= Haboudane et al. (2004), 9=Liu and Huete (1995), 10=Lichtenhaler et al. (1996), 11=Vogelmann et al. (1993), 12=Vogelmann et al. (1993), 13=Gitelson and Merzlyak (1997), 14=Haboudane et al. (2002), 15=Zarco-Tejada (1998), 16=Peñuelas et al. (1995), 17=Carter (1994 & 1996), 18=Datt et al. (1998), 19=Gitelson et al. (2003, 2006), 20= Merzlyak et al. (1999), 21= Lichtenhaler et al. (1996), 22=Chappelle et al. (1992), 23=Blackburn (1998), 24=Blackburn (1999), 25=Gamon et al. (1992), 26=Hernández-Clemente et al. (2011), 27=Gamon et al. (1993), 28=Zarco-Tejada et al. (2013), 29=Garrity et al. (2011), 30=Zarco-Tejada et al. (2000), 31=Gitelson et al. (2000), 32=Calderón et al. (2013), 33=Zarco-Tejada et al. (2005), 34=Zarco-Tejada et al. (2012), 35=Lichtenhaler et al. (1996), 36=Mahlein et al. (2013).

To precisely and accurately calculate spectra and derived vegetation indices for all trees surveyed in the field, each of the 293 trees were identified one by one in the imagery using the coordinates already recorded in situ by hand-held GPS devices. For each tree, image values were then extracted according to their delineated crowns, and averaged to provide a per-tree record of spectral characteristics. From these values, the aforementioned indices were calculated for each surveyed tree, as well as for the 30 apparently healthy trees.

5.4. Statistical analyses

Statistical analyses first provided an overall measure of the spectral dissimilarity between different levels of canopy decline through an analysis of variance (one-way ANOVA). Additional tests were then carried out to establish **which spectral indices could**

1) **distinguish apparently healthy trees from those showing some level of canopy decline**, considering defoliation, discolouration, and canopy die-off separately. Because we identified the apparently healthy trees from the imagery rather than in the field, there is some uncertainty regarding their crown condition. Therefore, we repeated the test to compare the 40 field-surveyed trees with the lowest level of canopy die-off (< 1 %) with those with higher levels of canopy die-off. As very few trees with the lowest classes of defoliation and discolouration (4 and 1 trees, respectively) were included in the field survey, this back-up test was not systematically carried out for these decline indicators.

2) **distinguish apparently healthy trees from those showing canopy decline, considering the different canopy decline levels individually**.

We used Dunnett's two-tailed t-test to investigate these issues, as it is designed to compare multiple levels of a phenomenon (in our case, levels of canopy decline) with a single control-level of the phenomenon (in our case, healthy canopies). The test accounts for the fact that, as more comparisons are made, the likelihood of one incorrectly showing a significant result (type I error) increases. The t-tests were statistically considered at $\alpha = 0.05$, implying that the chance of wrongly assigning detection ability was less than 5%.

5.5. Flight cost simulation

The distribution of coniferous forests and trees in the buffer zone is spatially very heterogeneous. As a result, some contiguous areas of coniferous forest can be imaged using a single aircraft flight line, while other forest areas can only be reached by long flights over non-forested areas. To illustrate the practical and financial implications of this for airborne surveying of the buffer zone, we calculated the shortest flight path required to cover a range of fractions of the coniferous forest in an 858 km^2 section of the buffer zone near Castelo Branco, Portugal. The flight simulations assumed a swath width of 1 km, and did not account for the location of airports. Moreover, the simulation assumed that the exact location of all coniferous tree stands is as described in the Copernicus high-resolution forest layer, which shows 101 km^2 of coniferous tree stands in the analysed section of the buffer zone.

6. Results

6.1. Tree crown delineation

To delineate the tree crowns, an operator visually inspected the imagery collected, on which he marked the centre of individual tree crowns A region growing algorithm was then developed to estimate the extent of the tree crowns around each of the points (*Figure 7*). The algorithm identified an area that a) was spectrally homogenous, b) did not contain any holes, and c) did not exceed the user-defined maximum tree-crown diameter. To identify this area, the algorithm started with a small cluster of pixels around the point identified by an operator, the size of which was determined by a user-defined minimum tree-crown diameter, and then evaluated whether each pixel adjoining the cluster was spectrally similar to the cluster. If so, the pixel was added to the cluster and the procedure continued. This procedure iteratively grows an area of spectrally similar pixels from the user-defined starting point. Any holes in the estimated crown were filled using mathematical morphological operations. Spectral similarity was evaluated for each iteration using the Mahalanobis distance: a measure of similarity of a point (in this case, a pixel at the edge of the crown) to a set of other points (in this case, the crown), in a multidimensional space (in this case, the space defined by the different image bands).

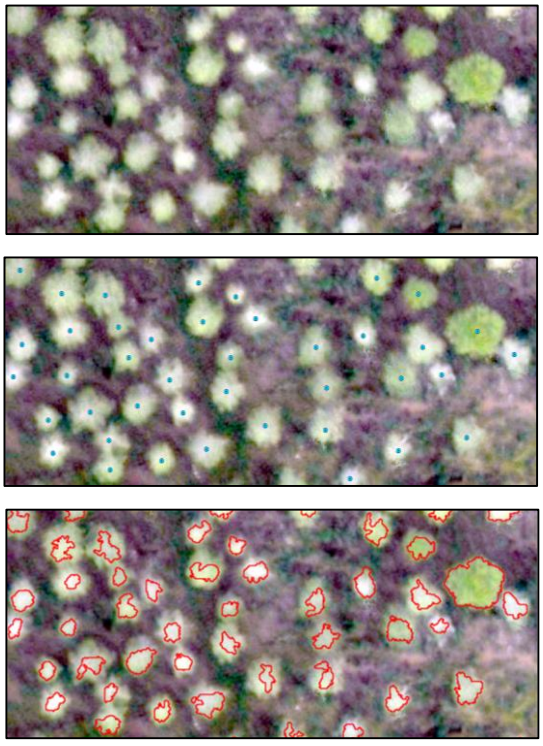

Figure 7. Example of crown-delineation procedure, which starts from very high resolution images (e.g. colour imagery of 11cm resolution, top panel), and points located inside tree crowns (blue dots in middle panel), and estimates the extent of the tree crown (red lines in bottom panel) using a region growing algorithm that progressively evaluates the area surrounding each point, to outline an area of homogenous colour that fits the user-defined shape and size characteristics of tree crowns. The depicted part of the Monte de Granadilla Forest measures 60 m across.

6.2. Spectral analyses

6.2.1. Colour imagery

The red, green and blue bands of the colour images and their ratios that included the green band helped to detect the presence of canopy decline, since significant ($P<0.05$) changes in symptomatic trees were detectable when compared with healthy trees. Moreover, many of these indices could help detect the decline at each of the decline severity levels.

Spectral index	F	*P*	All	In. 0	In. 1	In. 2	In. 3	In. 4	In. 5
					Defoliation				
R	25.69	<0.0001	X		X	X	X	X	X
G	13.55	<0.0001	X		X		X	X	X
B	25.87	<0.0001	X		X	X	X	X	X
R/G	87.06	<0.0001	X	X	X	X	X	X	X
R/B	8.87	<0.0001	X					X	
G/B	92.08	<0.0001	X	X	X	X	X	X	X
					Discolouration				
R	24.11	<0.0001	X		X	X	X	X	X
G	12.84	<0.0001	X		X	X	X	X	X
B	23.84	<0.0001	X		X	X	X	X	X
R/G	78.81	<0.0001	X	X	X	X	X	X	X
R/B	7.77	<0.0001	X					X	
G/B	84.38	<0.0001	X	X	X	X	X	X	X
					Canopy die-off				
R	26.3	<0.0001						--	
	2.59	0.037						--	
G	12.92	<0.0001	X	X	X	X		--	X
	2.84	0.025		*r-*				--	
B	26.74	<0.0001	X	X	X	X		--	X
	0.5	0.739		*r-*				--	
R/G	94.95	<0.0001	X	X	X	X	X	--	X
	0.17	0.954		*r-*				--	
R/B	13.65	<0.0001	X	X	X	X	X	--	
	16.42	<0.0001		*r-*				--	X
G/B	111	<0.0001	X	X	X	X		--	X
	26.29	<0.0001		*r-*			X	--	X

Table 6. Statistical analysis of the ability of colour image data acquired on 20/11/2014 to distinguish between healthy trees and those displaying canopy decline. Columns F and P give the F-statistic and associated significance level, respectively, for the one-way ANOVA evaluating the differences between all canopy decline classes, including the apparently healthy trees. The 'All' column indicates whether apparently healthy trees differed from trees with canopy decline, regardless of the level of decline. Statistically significant tests are denoted by an 'X'. Columns In. 0 to In. 5 indicate whether trees with individual intervals of canopy decline (sensu Table 1) differed significantly from apparently healthy trees. For Canopy die-off, the same tests used Canopy die-off interval 0 to represent healthy trees (indicated by r-). Intervals of canopy decline with no observations and irrelevant tests are indicated by --.

6.2.2. False-Colour / Near-Infrared (FCNI) imagery

The green, red and infrared bands of the FCNI imagery and their ratios showed significant ($P<0.05$) changes in symptomatic trees compared with apparently healthy trees. Moreover, most of these bands helped detect the decline at each of the decline levels.

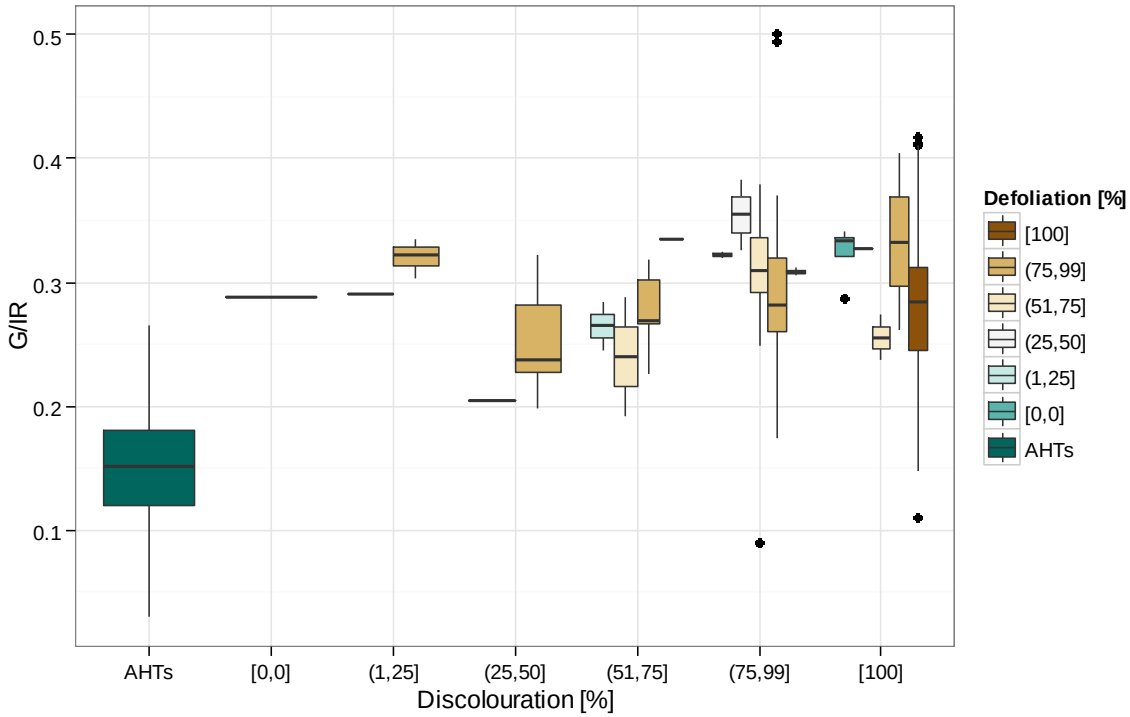

Figure 8. Index of Green (G) over Infrared (IR) radiance derived from false-colour / near-infrared (FCNI) imagery for apparently healthy trees (AHTs) and trees displaying increasing levels of canopy discolouration and defoliation. Boxes extend between the 25 and 75% quantiles of the index, and show the median.

Spectral index	F	*P*	All	In. 0	In. 1	In. 2	In. 3	In. 4	In. 5
Defoliation									
R	5.77	<0.0001	X		X		X	X	X
G	12	<0.0001	X		X	X	X	X	X
IR	6.55	<0.0001	X	X				X	X
R/G	26.19	<0.0001	X	X	X	X	X	X	X
R/IR	15.92	<0.0001	X	X	X	X	X	X	X
G/IR	34.14	<0.0001	X	X	X	X	X	X	X
Discolouration									
R	5	<0.0001	X					X	X
G	11.91	<0.0001	X		X	X	X	X	X
IR	5.31	<0.0001	X				X	X	X
R/G	25.27	<0.0001	X		X	X	X	X	X
R/IR	17.51	<0.0001	X		X	X	X	X	X
G/IR	34.84	<0.0001	X	X	X	X	X	X	X
Canopy die-off									
R	5.19	<0.0001	X	X	X	X		--	X
	1.06	0.375		*r-*				--	
G	13.99	<0.0001	X	X	X	X		--	X
	2.48	0.044		*r-*				--	
IR	6.27	<0.0001	X	X	X			--	X
	1.75	0.140		*r-*				--	
R/G	30.99	<0.0001	X	X	X	X		--	X
	2.98	0.019		*r-*				--	
R/IR	19.03	<0.0001	X	X	X	X		--	X
	0.85	0.494		*r-*				--	X
G/IR	40.46	<0.0001	X	X	X	X		--	X
	1.52	0.197		*r-*				--	

Table 7. Statistical analysis of the ability of false-colour / near-infrared image (FCNI) data acquired on 28/01/2015 to distinguish between healthy trees and those displaying canopy decline. Columns F and P give the F-statistic and associated significance level, respectively, for the one-way ANOVA evaluating the differences between all canopy decline classes, including the apparently healthy trees. The 'All' column indicates whether apparently healthy trees differed from trees with canopy decline, regardless of the level of decline. Statistically significant tests are denoted with an 'X'. Columns In. 0 to In. 5 indicate whether trees with individual intervals of canopy decline (see Table 1) differed significantly from apparently healthy trees. For Canopy die-off, the same tests were applied using Canopy die-off interval 0 to represent healthy trees (indicated with r-). Intervals of canopy decline with no observations and irrelevant tests are indicated by --.

6.2.3. Hyperspectral imagery

All of the tested hyperspectral indices detected statistically significant differences between the different canopy status classes when the apparently healthy trees were included in the analysis (P_{ANOVA} < 0.0001 for all indices). Statistically significant differences between the apparently healthy trees and the ensemble of surveyed trees were found for all indices and canopy decline measures, except for the BGI1 index, which did not differ for trees showing defoliation or canopy die-off.

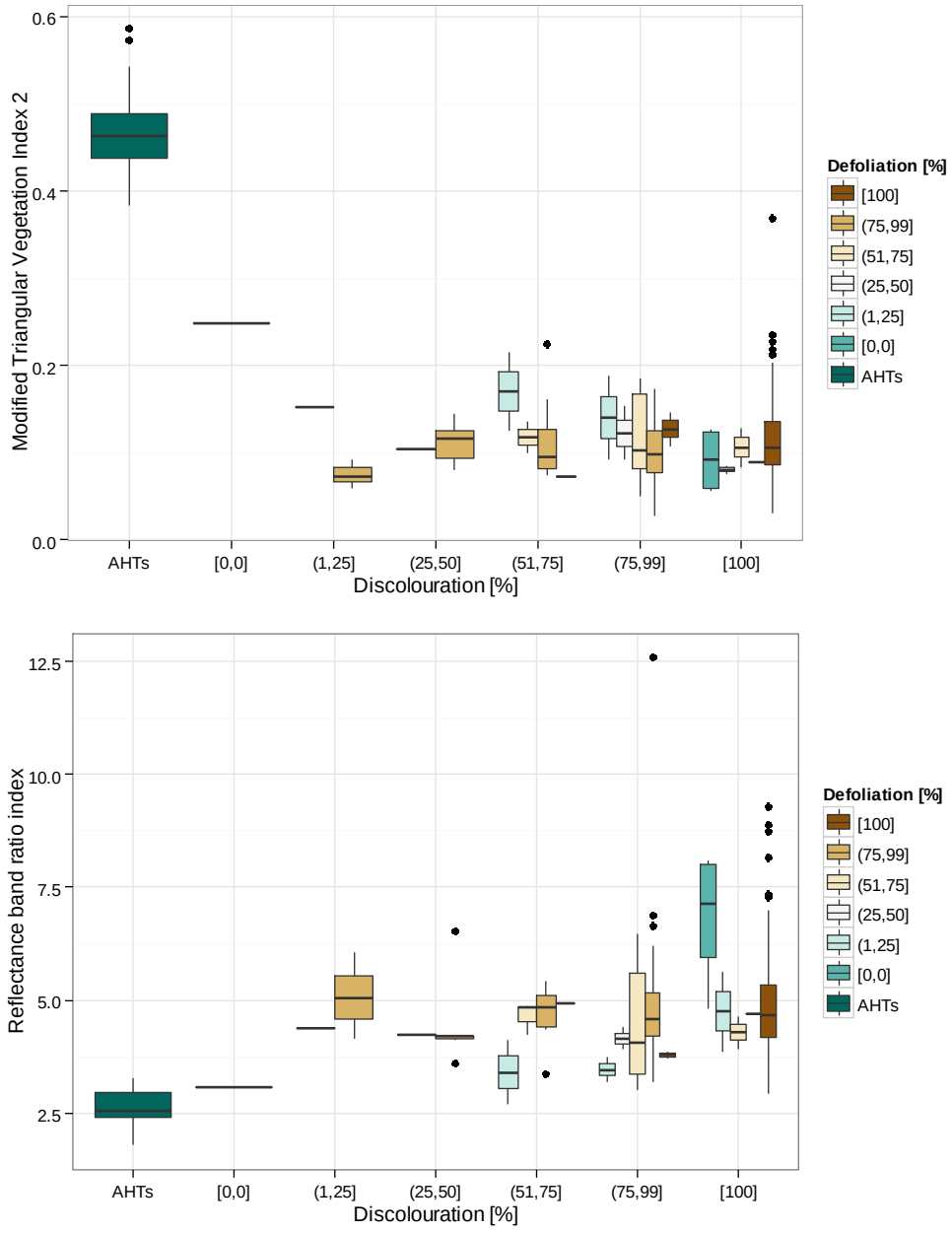

Figure 9. (Top) Modified Triangular Vegetation Index 2 (Haboudane et al., 2004, doi:10.1016/j.rse.2003.12.013) and (bottom) Reflectance band ratio index (Datt et al., 1998, Remote Sensing of Environment) derived from hyperspectral data for apparently healthy trees (AHTs), and trees displaying increasing levels of canopy discolouration and defoliation. Boxes extend between the 25 and 75% quantiles of the index, and show the median.

Spectral indices responded non-linearly to discolouration: many indices distinguished between apparently healthy trees and those showing any canopy decline (e.g. the Modified Triangular Vegetation Index 2 in *Figure 9*). At the same time, the spectral indices did not obviously differ between surveyed trees with different levels of discolouration. This is partly because trees that showed greater discolouration tended to also show greater defoliation, where defoliation accounts both for leaves that have been shed and those that are brown and dead but still on the branches. However, when more than half of the canopy was discoloured, many indices could detect increasing levels of canopy defoliation. Sample sizes were too small to evaluate whether this was also the case at lower discolouration levels. When the entire canopy was discoloured, sensitivity to defoliation was apparently lost (e.g. MTVI2, PRIM4), or even reversed, in some cases causing canopies that are completely discoloured but not at all defoliated to show the most extreme spectral indicex values (e.g. Reflectance band ratio index in Figure 9).

6.2.4. Thermal imagery

Crown temperature values extracted from the collected airborne thermal imagery helped to distinguish trees with severe levels of canopy decline from apparently healthy trees.

Flight	F	*P*	All	In. 0	In. 1	In. 2	In. 3	In. 4	In. 5
Defoliation									
1	1.11	0.358					X	X	X
2	3.35	0.003					X	X	X
Discolouration									
1	0.92	0.479						X	X
2	3.44	0.003						X	X
Canopy die-off									
1	0.82	0.534	X	X	X			--	X
2	3.47	0.005		X	X			--	X
1	0.178	0.911		*r-*				--	
2	0.157	0.925		*r-*				--	

Table 8. Statistical analysis of the ability of thermal image data acquired on 02/12/2014 (Flight 1) and 28/01/2015 (Flight 2) to distinguish between healthy trees and those displaying canopy decline. Columns F and P give the F-statistic and associated significance level, respectively, for the one-way ANOVA carried out to evaluate the differences between all canopy decline classes, including apparently healthy trees. The 'All' column indicates whether apparently healthy trees differed from trees with canopy decline, regardless of the level of decline. Statistically significant tests are denoted by an 'X'. Columns In. 0 to In. 5 indicate whether trees with individual intervals of canopy decline (see Table 1) differed significantly from apparently healthy trees. For Canopy die-off, the same tests used Canopy die-off interval 0 to represent healthy trees (indicated by r-). Intervals of canopy decline with no observations and irrelevant tests are indicated by --.

6.3. Mapping canopy decline

Canopy decline can be mapped by evaluating the condition of each delineated crown based on spectral analysis, and representing this evaluation in a cartographic system. The resulting maps (e.g. *Figure 10*) provide an overview of forest health and can help ground crews to prioritise forest management interventions. Furthermore, the maps, whether provided in hard copy or (interactive) digital format, can be used as a tool for these ground crews to provide feedback on the quality of the maps, indicating where the maps correctly and incorrectly identified declining and unhealthy trees. As such, the maps provide a critical medium for the exchange of information between the remote sensing data analysis and ground observations. The maps can help to optimise ground interventions, and to further improve the methods used in remote sensing analysis.

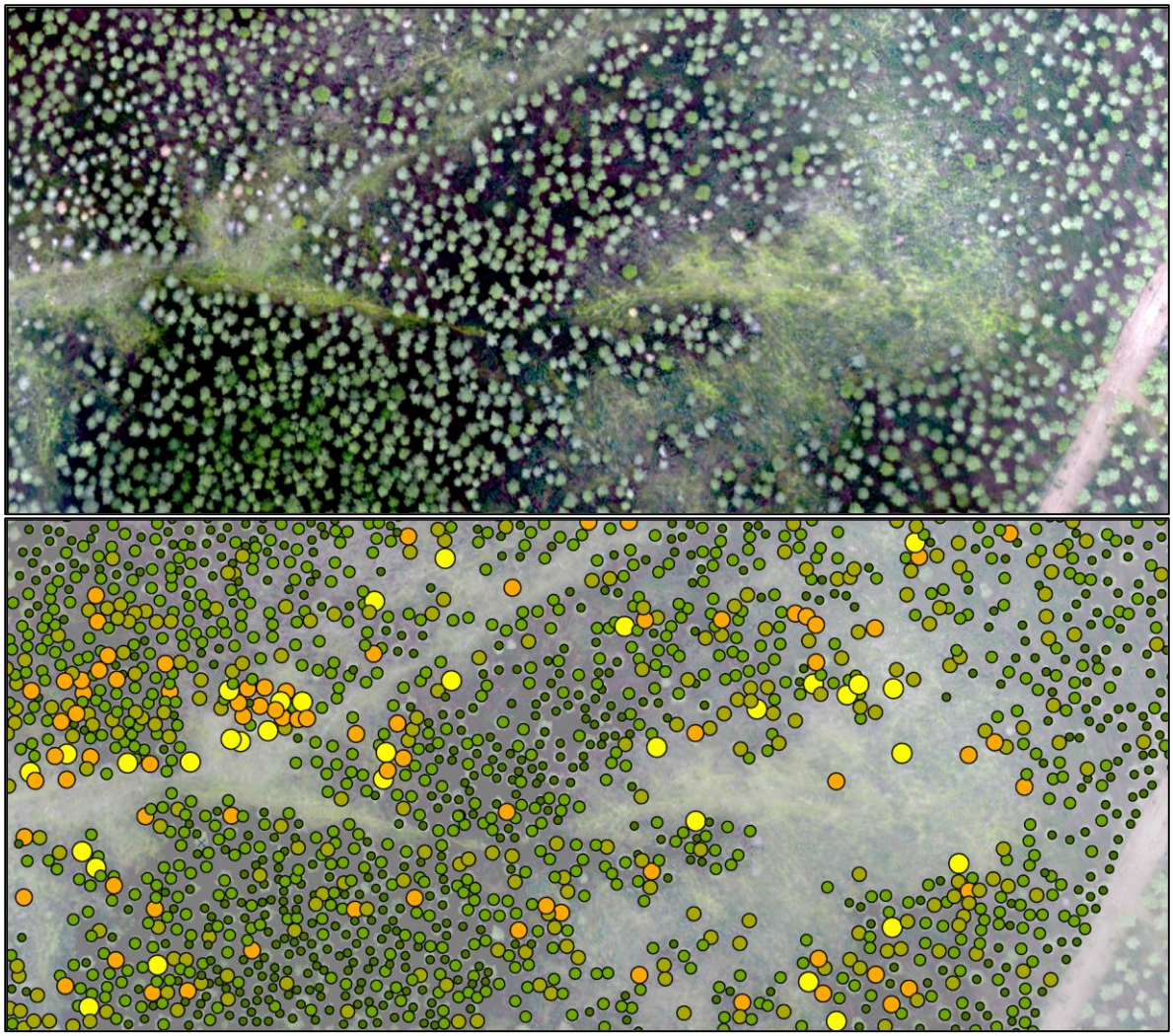

Figure 10. Example of the colour imagery collected over the Monte de Granadilla forest (top), and a tree crown condition indicator based on spectral information in the imagery (bottom): Larger symbols indicate trees where the imagery show increasing levels of canopy decline, and which would be prioritised in a field campaign aimed at inspecting or removing trees in poor health. Maps such as this one can be shared in hard copy or digitally with teams working in the field, and can also be used for feedback to improve tree crown condition mapping based on remote sensing. The depicted area measures 360 m across.

7. Prospects for monitoring declining trees using remote sensing

7.1. Image resolution requirements

The prevalence of pine trees with projected crown diameters of 2 m or less dictates the use of very high resolution imagery for tree-level forest monitoring in the context of the Pine Wood Nematode threat. Image data from civilian sensors on Earth Orbiting satellites provide panchromatic images up to circa 50 cm resolution, and multispectral images down to ca. 1.5 m resolution. While these images might help detect changes at the stand level, they do not capture sufficient spatial detail for the exhaustive mapping or monitoring of individual tree crowns. By contrast, imaging campaigns using airborne sensors have the advantage of being able to acquire data at the spatial resolution required for the identification of all canopy crowns. Furthermore, the relatively coarse resolution of satellite compared to airborne images hinders the precise spatial alignment of images acquired on different dates, which is required to detect changes in individual tree crowns over time.

While Remotely Piloted Aircraft Systems (RPAS) are rapidly dropping in price and gaining in sophistication, large-area imaging requires relatively large and heavy RPAS in order to avoid frequent refuelling stops. Such RPAS are subject to legal restrictions with regard to weight and flights beyond the line-of-sight of the RPAS' operator, currently limiting their usability to image large areas. In addition, even the larger RPAS for Earth imaging have a smaller range than manned aircraft, can carry smaller payloads (i.e. sensors), and are more affected by adverse weather conditions. Therefore, given the size of the buffer zone and current civilian technology and aviation rules, it would be extremely difficult to map the zone using RPAS.

That said, RPAS could provide cost-efficient complements for the (re-)imaging of smaller or remote forest areas (particularly if the RPAS can be operated by forest management crews), and images obtained by the RPAS can be visually reviewed in near real-time. In addition, RPAS could be of great value for the intense monitoring of areas where the risk of PWD is studied through experiments. In such cases, their ease of deployment would allow the frequent surveillance of experimental and control plots in order to evaluate the detectability of symptoms as they progress in controlled settings.

[REC.1] To provide a detailed record of individual coniferous tree crowns in the buffer zone, the area should be imaged in colour at 20 cm or higher spatial resolution from manned airborne platforms.

[REC.2] Images acquired for forest monitoring in the context of the PWN emergency should be of very high quality in terms of georegistration to ensure that, once repeat imagery is available, changes can be detected as close to the individual crown level as possible.

Once the high quality georegistration of images is assured, and individual tree crowns are delineated and evaluated for PWD using aerial images, the use of lower resolution but more frequent (satellite) data for canopy change detection should be researched. In particular, new constellations of high resolution satellites (e.g. Skybox) now provide circa 1.5 m resolution colour images at weekly intervals. While these data are too spatially coarse for tree crown delineation, their high temporal resolution could permit the detection of rapid changes in canopy condition in small groups of trees earlier than the once- or twice-yearly airborne campaigns.

7.2. Spectral band optimisation

Spectral indices calculated from colour and FCNI images, combined with visible inspection of the images, indicated that broad-band visible imagery can be used to detect many (particularly severe) cases of canopy decline.

However, some spectral indices calculated using the hyperspectral image data showed greater ability to distinguish between AHTs and trees with canopy decline, and/or a tendency to increase steadily with increasing levels of canopy decline. Hyperspectral image acquisition over large areas generates a large volume of data that is very time-consuming to process and partly redundant. Multispectral sensors can be tuned to collect data in circa six narrow spectral bands, at lower acquisition and processing costs. Based on our findings, measurements around the following six wavelengths can be used to calculate a range of spectral indices that show potential to detect progressive stages of canopy decline: 450 nm, 490 nm, 670 nm, 710 nm, and 800 nm. These indices include the two Reflectance band ratio indices, the (re)Normalized Vegetation Index, and a blue-green index.

[REC. 3] In an attempt to detect lower levels of canopy decline, a multispectral narrow-band sensor should image areas of interest from the same aircraft and at the same time as broad-band colour images are acquired, at the highest spatial resolution achievable.

The thermal data acquired during this study helped identify trees showing severe levels of canopy decline. As the data for this study was collected during the winter months, it was poorly suited to fully evaluate the potential of thermal imagery for the detection of early stages of canopy decline. In summer, when the atmosphere is hot and dry, leaves lose greater amounts of water during photosynthesis, which has a cooling effect on the canopy. The obstruction of the xylem, e.g. by pine wood nematode or other wilt-causing agents, impedes this cooling mechanism, causing canopy temperatures to rise. The difference between healthy and unhealthy trees is expected to be greatest when atmospheric water demand is high, and could theoretically be detectable before the canopy displays visible wilt symptoms

[REC. 4] Thermal imaging of pine forests with early stages of canopy decline should be conducted in summer during times of high atmospheric water demand, in order to evaluate in more detail the ability of thermal images to detect canopy decline earlier than optical imagery.

7.3. Image processing requirements

Because all the spectral characteristics of declining trees are not known a priori, it is difficult to detect all trees in imagery purely based on their spectral characteristics, which also runs the risk that some trees, and specifically declining ones, go unidentified. Therefore, extensive and time-consuming visual validation of tree detection methods, be it through photointerpretation or automated algorithms, will be required.

The mapping of individual tree crowns using very high resolution imagery permits the inspection of individual trees for symptoms of decline. It also is valuable for the generation of canopy cover data, which can inform the analysis of spatially coarser, but more frequent, image data. Most importantly, it allows for the tracking of the canopy status of individual trees over time. Once repeat imagery is available, the spectral characteristics of each tree

crown can be compared to earlier observations, as well as to those of nearby trees. Trees recently affected by PWD are expected to show spectral changes that are not seen in surrounding trees. In other words, when repeat imagery is available, trees showing rapid canopy decline can increasingly be detected because of relative rather than absolute spectral characteristics. As such, the use of repeat observations shifts the demands on the image data from the radiometric to the geographic domain. This requires that images are at least geographically aligned with each other with very high precision. Better still, images should be orthorectified precisely, and registered in a cartographic reference system.

[REC. 5] To attain the highest cartographic precision possible in collected imagery, the best available high resolution digital elevation models and existing catalogues of aerial orthophotographs of the area to be surveyed should be used for the orthorectification and geometric rectification of newly acquired imagery.

Using repeat imagery to monitor the buffer zone at or near the tree level further allows for an assessment of the rate at which symptoms develop, which can help distinguish between trees showing rapid canopy decline, and those that have been in poor canopy condition, or even dead, for longer periods of time. This distinction could greatly help to inform forest management operations as they have different roles in the PWN lifecycle, e.g. Pine trees that have been dead for two years do not provide a breeding habitat for *Monochamus* beetles.

7.4. Information exchange with in situ operations

Results from the analysis of remote sensing data should be communicated to interested parties in map format, providing a spatial representation of canopy condition both at regional scales, e.g. summarised at the level of administrative units, and at very local scales, e.g. mapping the estimated condition of canopy condition at the level of individual trees or tree stands. The latter maps should be shared in digital format and through an online web mapping service so that they can be incorporated into geographical information systems and used to plan forest management activities. As such, the maps can form a medium for information exchange between the coordinators of the remote-sensing-based survey and national or regional authorities in charge of field surveys. Competent authorities carrying out field inspections could use the map to plan their activities and could also perform in situ validation of the maps. This feedback on the performance of the remote-sensing-based survey is crucial in order to continuously test and refine algorithms for the detection of canopy decline in remote sensing imagery.

Basic information, such as updates from competent authorities on tree fellings, will help keep the remote sensing analysis focused on extant trees. Up-to-date access to field observations on canopy status is critical, however, as PWD symptoms develop rapidly, and ground observations for the pilot study did not include completely healthy trees but were biased towards trees with severe symptoms of decline, and ignored trees with single discoloured branches – as expected in the early stages of PWD. Algorithm refinements should incorporate information on the causes of canopy decline, particularly whether laboratory analyses indicated the presence of PWN, to research the remote-sensing-based attribution of canopy decline in pines.

[REC. 6] Output from remote sensing analyses should be made available in GIS-compatible digital formats. Up-to-date information from field observations, laboratory

analyses, and felling operations should be accessible during the analysis of remote sensing imagery so that output can be validated, and methods progressively refined.

7.5. Long-term cost considerations

The flight simulation shows how the cost of monitoring coniferous forest from aircraft increases rapidly as the forest area to be covered approaches 100%. This occurs because, while a significant fraction of the coniferous forest area grows in very large contiguous stands, a smaller fraction occurs in small forest stands that are distant from larger ones. Imaging these smaller areas requires the aircraft to fly large distances between forest areas, thereby incurring disproportionate costs. For the 858 km^2 area near Castelo Branco considered in the simulations, this effect of diminishing returns on investment is particularly large once 80% of the coniferous forest has been imaged (*Figure 11*). As a result, imaging all coniferous forest areas would be twice as costly as imaging the 91% most accessible portion.

Similarly, reaching smaller, remote forest patches imposes additional costs on field surveys. Even if they were available at sufficiently fine resolution, it is not cost-efficient to order very high resolution satellite images for these forest patches, since vendors of such data commonly set minimum areas (e.g. 25 km^2) for individual orders. However, while they are costly to survey, regardless of the method employed, small remote forest areas might be more easily and confidently surveyed in the field compared to larger ones, simply because the number of trees to inspect is smaller. Conversely, surveying all the trees in a large forest is challenging using field methods, but comparatively cheap using remote sensing.

This analysis assumes that the presence of coniferous trees is known before the image acquisition, based on pan-European forest type distribution maps which are now available at 25 m resolution. However, these maps do not show the presence of individual trees or very isolated small clusters of trees, and still have unknown error distributions. By contrast, halting the spread of PWN requires tree-level observations with very low omission rates during the detection of canopy decline, and requires the generation of very precise tree distribution maps.

[REC. 7] An initial phase of operational monitoring of the PWN buffer zone should aim to obtain wall-to-wall imaging of priority areas, in order to allow for the mapping of all individual coniferous tree stands in those areas. In a second phase of operational monitoring, once individual trees have been mapped, flight paths could be planned together with complementary ground surveys, to optimise the cost efficiency of the monitoring exercise.

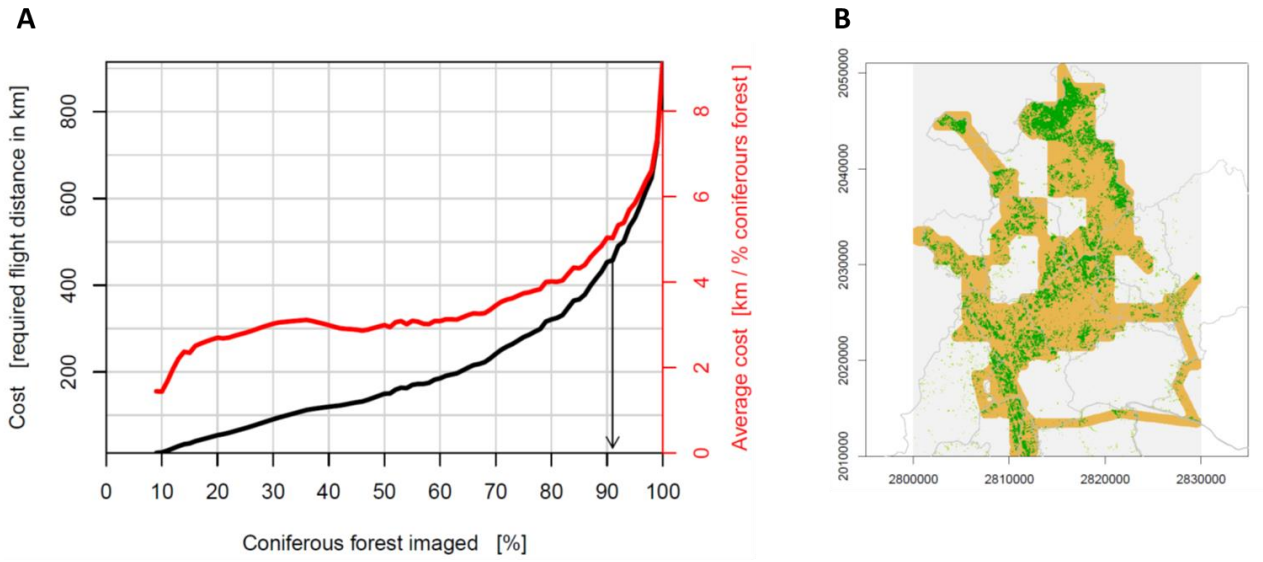

Figure 11. (A) Simulated cost of an aircraft flying over progressively larger fractions of the coniferous forest in an 858 km² section of the buffer zone. Coniferous forest in the selected area covers an estimated 101 km², and the cost analysis assumes that the aircraft observations have a swath width of 1 km. The black line indicates the total cost of imaging progressively larger fractions of the coniferous forests, while the red line depicts the average cost per coniferous forest area imaged. The arrow points to the fraction of coniferous cover that can be imaged at half the cost of imaging all coniferous forest areas (in casu 91%). (B) Theoretical flight path (in orange) that covers 91% of the coniferous forest (green) in the section of buffer zone nearest to Castelo Branco. Grey lines delineate the administrative areas that fall within the buffer zone.

7.6. Suggested next steps

This pilot study established that it is feasible to reliably detect pine trees showing severe canopy decline using remote sensing of a landscape similar to that found in the PWN buffer zone. It provides clear recommendations for more operational remote-sensing-based forest monitoring activities in the context of PWN, as well as for continued research into cost-efficient methods. At 2.2 Mha, the PWN buffer zone is large, and an exceptionally large volume of image data needs to be acquired and processed to monitor it exhaustively for declining trees. We therefore suggest that the implementation of tree decline detection techniques be further developed, following the recommendations from the pilot study, over an area significantly larger than that of the pilot study (from 10 000 to 100 000 ha), but still smaller than the entire buffer, so as to reduce the significant risk of scaling up the operations too quickly. The area for a next phase of monitoring should be chosen in a priority region of the buffer zone, e.g. closest to the current PWN distribution, in order for results to have immediate forest management value.

8. Towards a versatile remote-sensing-based forest health monitoring system against tree pests

Forests are critical natural resources, in Europe and globally. In Europe, forest management is a pillar of the bioeconomy, supplying about half of the EU's renewable energy consumption and a wide range of ecosystem services. Globally, forests provide an annual net sink for 1.1 Pg of carbon in the atmosphere, an amount equivalent to about 1/8th of annual CO_2 emissions from fossil fuel use and cement production.

In step with increasing global trade, exotic tree pests now pose a new and very real threat to forests in Europe. Tree pests can cause rapid and widespread damage to forests, reducing their economic value and prospects, and their role in mitigating climate change. Sustaining the economic and societal benefits of forests requires managing them in such a way that they are resilient to disturbances and climate change.

The ongoing outbreak of PWN in Europe was the impetus for this pilot study. Since it was first detected in Portugal in 1999, exceptional measures have been taken to curtail the spread of PWN, financed in part by the European Commission. Other tree pests present similar threats to forest resources in Europe; for example, in October 2013 the bacterium *Xylella fastidiosa* was first observed in Europe, more precisely in Southern Italy, where it has since been associated with a rapid decline in the health of olive trees throughout the region of Apulia.

The technical challenges to detecting trees with declining canopies, detailed in the present study, are not unique to the PWN case. Indeed, they can form the basis for a versatile remote-sensing-based toolkit to monitor forest health in the fight against any tree pest. Several Member States are currently carrying out research to detect pest disturbances in forest stands. However, given the extent and rate at which pests are currently spreading, and the threat of pests spreading from one Member State to another, a pan-European early warning system for forest health would have significant benefits. Such a system should be rapidly deployable, capable of incorporating extant remote sensing data and field observations, and point towards necessary additional data acquisitions. The system should be able to process these data to provide decision makers at multiple administrative levels with readily usable output in the form of maps and summaries of the state of a pest outbreak.

9. Acronyms

AHL	**APPARENTLY HEALTHY TREE**
DEM	Digital elevation model
DSLR	Digital Single Lens Reflex
FCNI	False-Colour / Near-Infrared
GIS	Geographical Information System
IGN	Instituto Geográfico Nacional
MS	Multispectral
PAN	Panchromatic
PRI	Photochemical Reflectance Index
PWD	Pine Wilt Disease
PWN	Pine Wood Nematode
REC	Recommendation
RGB	Red, Green, and Blue
RPAS	Remotely Piloted Aircraft Systems

Table 9. Acronyms used in this report (acronyms of spectral indices listed in Table 5 are not repeated here).

10. Acknowledgements

The authors would like to thank Gerardo Sánchez Peña of Spain's Ministerio de Agricultura, Alimentación y Medio Ambiente, and Eudaldo González Rosa for their help in selecting the pilot study site, and the coordination of the field measurements, respectively.

European Commission
EUR 27290 EN – Joint Research Centre – Institute for Environment and Sustainability

Title: **The feasibility of detecting trees affected by the Pine Wood Nematode using remote sensing**

Authors: Pieter S. A. Beck, Pablo Zarco-Tejada, Peter Strobl, Jesús San Miguel

Luxembourg: Publications Office of the European Union

2015 – 32 pp. – 21.0 x 29.7 cm

EUR – Scientific and Technical Research series – ISSN 1831-9424 (online)

ISBN 978-92-79-48946-4

doi: 10.2788/711975

LB-NA-27290-EN-N

JRC Mission

As the Commission's in-house science service, the Joint Research Centre's mission is to provide EU policies with independent, evidence-based scientific and technical support throughout the whole policy cycle.

Working in close cooperation with policy Directorates-General, the JRC addresses key societal challenges while stimulating innovation through developing new methods, tools and standards, and sharing its know-how with the Member States, the scientific community and international partners.

Serving society
Stimulating innovation
Supporting legislation

doi: 10.2788/711975

ISBN 978-92-79-48946-4

Publications Office